

An Enhanced Formation Channel for Galactic Dual-Line Gravitational-Wave Sources: von Zeipel-Lidov-Kozai effect in Triples Involving Sgr A*

WEN-FAN FENG ,¹ TAN LIU ,^{2,3} YUN FANG ,^{4,5} YACHENG KANG ,^{6,1} BIN LIU ,⁷ AND LIJING SHAO ,^{1,8}

¹*Kavli Institute for Astronomy and Astrophysics, Peking University, Beijing 100871, China*

²*School of Fundamental Physics and Mathematical Sciences, Hangzhou Institute for Advanced Study, University of Chinese Academy of Sciences, Hangzhou 310024, China*

³*School of Physical Sciences, University of Chinese Academy of Sciences, Beijing 100049, China*

⁴*Institute of Fundamental Physics and Quantum Technology, Ningbo University, Ningbo 315211, China*

⁵*School of Physical Science and Technology, Ningbo University, Ningbo 315211, China*

⁶*Department of Astronomy, School of Physics, Peking University, Beijing 100871, China*

⁷*Institute for Astronomy, School of Physics, Zhejiang University, Hangzhou 310027, China*

⁸*National Astronomical Observatories, Chinese Academy of Sciences, Beijing 100101, China*

ABSTRACT

The dense Galactic Center environment is expected to host compact binary inspirals detectable by future space-borne gravitational wave (GW) observatories (e.g., LISA, TianQin, Taiji) in the millihertz band. Aided by information from these facilities, next-generation ground-based GW detectors (e.g., Cosmic Explorer, Einstein Telescope) can potentially capture gravitational radiation in the hectohertz band from rapidly spinning neutron star (NS) components in such binaries. These Galactic Center systems are thus anticipated to act as dual-line (i.e., low-frequency inspiral and high-frequency spin) GW sources. However, the formation channels of these systems remain largely unexplored. In this *Letter*, we propose that the von Zeipel-Lidov-Kozai (ZLK) effect can enhance the formation of dual-line GW sources in hierarchical triples involving the Galactic supermassive black hole, Sgr A*. We show that ZLK-driven oscillations in the eccentricity and inclination of the inner binary can modulate the GW emission from both the binary inspiral and the individual NS spins. This effect boosts the expected dual-line source count by a factor of ~ 3 , from rare to $\mathcal{O}(1)$ in 4 years, making dual-line observations substantially more probable. Our results demonstrate that the ZLK effect provides an important formation channel for Galactic dual-line GW sources.

Keywords: Gravitational wave sources (677) — Neutron stars (1108) — Supermassive black holes (1663) — Galactic center (565)

1. INTRODUCTION

The groundbreaking detection of gravitational waves (GWs) has opened an unprecedented window for observing the cosmos (B. P. Abbott et al. 2016a, 2017). With their distinct, high-sensitivity frequency bands, next-generation ground-based detectors (e.g., Cosmic Explorer, V. Srivastava et al. (2022); Einstein Telescope, M. Punturo et al. (2010)) and space-borne observatories (e.g., LISA, P. Amaro-Seoane et al. (2017); TianQin, J. Luo et al. (2016); Taiji, W.-R. Hu & Y.-L. Wu (2017)) will facilitate the detection of low-frequency inspiral and high-frequency spin (dual-line⁹) gravitational radiation from Milky Way neutron star (NS) binaries, including NS–NS, NS–black hole (NS–BH), and NS–white dwarf (NS–WD) systems. This dual-line signal comprises two components: millihertz-band radiation from the binary inspiral, and hectohertz-band radiation from a rapidly spinning NS component. Population simulation and GW waveform modeling of isolated NS–NS systems in the Galactic field, treated as dual-line sources, have been performed in previous works (W.-F. Feng & L. Shao 2025; W.-F. Feng et al. 2025, 2023b). Observations of such

Email: fengwf@pku.edu.cn, lshao@pku.edu.cn

⁹ Dual-line originally refers to GW emission at $2f_{\text{orb}}$ and $2f_s$ from circular-orbit inspiralling NS binaries (T. M. Tauris 2018), where f_{orb} and f_s denote the orbital frequency and NS spin frequency, respectively. For eccentric-orbit binaries and precessing NS components, both the low- and high-frequency GW emission exhibit multiple harmonics; we nevertheless retain this terminology for simplicity.

systems would enable constraints on NS structural parameters (T. M. Tauris 2018; W.-C. Chen 2021; A. G. Suvorov 2021; W.-F. Feng et al. 2024; W.-F. Feng & L. Shao 2025), thereby helping to pin down the long-sought equation of state of NS matter.

The Galactic Center hosts Sagittarius A* (Sgr A*), the nearest known supermassive black hole (SMBH), with a mass of $\sim 4 \times 10^6 M_\odot$ (A. M. Ghez et al. 2005, 2008; S. Gillessen et al. 2009; A. Boehle et al. 2016; K. Akiyama et al. 2022a). Dominating the gravitational dynamics of its surroundings, Sgr A* provides a unique laboratory for testing gravity and stellar dynamics (e.g., A. M. Ghez et al. 2003; T. Alexander 2005; S. Gillessen et al. 2012; C. Hopman 2009; T. Alexander & O. Pfahl 2014; A. Hees et al. 2017; D. S. Chu et al. 2018; L. Shao et al. 2018; K. Akiyama et al. 2022b; Z. Hu & L. Shao 2024; J.-C. Yu et al. 2025). The dense environment at the Galactic Center likely harbors abundant stellar and compact binaries, many of which form triple systems with Sgr A*. Stability constraints favor a hierarchical configuration for most such systems: a tight inner binary orbited by a distant tertiary on a wider orbit, forming the outer binary. Gravitational perturbations from the distant tertiary (e.g., Sgr A*) drive periodic oscillations in the inner binary's orbital eccentricity and inclination via the von Zeipel-Lidov-Kozai effect (ZLK; H. von Zeipel 1910; Y. Kozai 1962; M. L. Lidov 1962; see S. Naoz 2016 for a review). This effect induces rich and complex dynamical processes in stellar evolution within the Galactic Center (e.g., A. P. Stephan et al. 2016). Studies of the ZLK effect have concentrated on stellar-mass BH-BH systems in galactic nuclei. The prospects for detecting ZLK-modulated GW signals with LISA have been assessed (B.-M. Hoang et al. 2019; L. Randall & Z.-Z. Xianyu 2019; A. M. Knee et al. 2024), while analytical frameworks for GW modeling from ZLK-driven inspiraling systems have been formulated (R. S. Chandramouli & N. Yunes 2022).

Despite large uncertainties in parameter settings and binary evolution, A. P. Stephan et al. (2019) modeled the dynamical evolution of binaries near Sgr A* under the ZLK effect, including tidal interactions, relativistic effects, and single/binary stellar evolution. Their simulations produced diverse outcomes, including compact binaries detectable as GW sources by LISA and Advanced LIGO (B. P. Abbott et al. 2016b). Incorporating ultra-stripped supernova explosions with reduced natal kicks, H. Wang et al. (2021) estimated that LISA could detect 0.4–4 NS-NS and 0.2–2 NS-BH systems within the Galactic Center's inner parsec, corresponding to merger rates of $\sim 0.3 \text{ Gpc}^{-3} \text{ yr}^{-1}$. These estimates are conservative, as they exclude additional dynamical processes like binary-single/binary-binary interactions (e.g., D. R. Rodriguez & B. Zuckerman 2012; F. Zhang et al. 2019; M. A. Sedda 2020) and single-single captures (e.g., R. M. O'Leary et al. 2009; D. Tsang 2013; B.-M. Hoang et al. 2020) that could enhance the compact binary population. For dual-line sources, assuming log-uniform outer-orbit distributions and a detection fraction of 20%–60% for rapidly spinning NS components (W.-F. Feng & L. Shao 2025), we predict only $\mathcal{O}(0.01 - 0.4)$ detectable systems within 100 AU over 4 years of combined observations. This suggests that the Galactic Center dual-line detections remain extremely challenging and unlikely with current expectations.

However, this pessimistic outlook is significantly altered when the ZLK effect is taken into account. In this *Letter*, we investigate dual-line GW sources from NS-NS systems in hierarchical triples involving Sgr A*, demonstrating that the ZLK effect can enhance detection rates by roughly threefold. Our dynamical analysis shows that ZLK oscillations dominate over general relativistic precession for typical NS-NS systems at the Galactic Center. We specifically model the GWs from the spinning NS components subject to the ZLK effect and map the detectable parameter space (equatorial ellipticity vs. spin period) accessible to Cosmic Explorer. The ZLK-induced eccentricity excitation facilitates dual-line signal formation, transforming detection count from $\mathcal{O}(0.01 - 0.4)$ to $\mathcal{O}(0.03 - 1)$ over 4 years and making dual-line observation in dense environments observationally promising. Throughout this paper, we adopt geometric units ($G = c = 1$).

2. DYNAMICAL TIMESCALES FOR GALACTIC CENTER TRIPLES

We consider a hierarchical triple system in the Galactic Center (see Fig. 1), consisting of an inner binary orbiting the Sgr A* of mass m_3 . As a representative case, we model the inner binary as an NS-NS system with a spinning primary component (mass m_1 , spin \mathbf{S}_1) and a non-spinning companion (mass m_2) (W.-F. Feng et al. 2023a). Our methodology extends straightforwardly to NS-BH systems. The inner and outer orbits are described by their respective semimajor axes (a_i, a_o) and eccentricities (e_i, e_o). The angular momenta of the inner and outer orbits are denoted by \mathbf{L}_i and \mathbf{L}_o , with their respective magnitudes L_i and L_o . The outer orbital plane is adopted as the reference plane, such that the outer orbital angular momentum is aligned with the Z -axis. The validity of this reference frame is justified by the dynamical timescale analysis presented below. The inclination angle ι_d is measured between \mathbf{L}_o and the vector towards detector \mathbf{D} , while ι_s is the angle between \mathbf{L}_o and primary spin \mathbf{S}_1 . The reference system is defined with

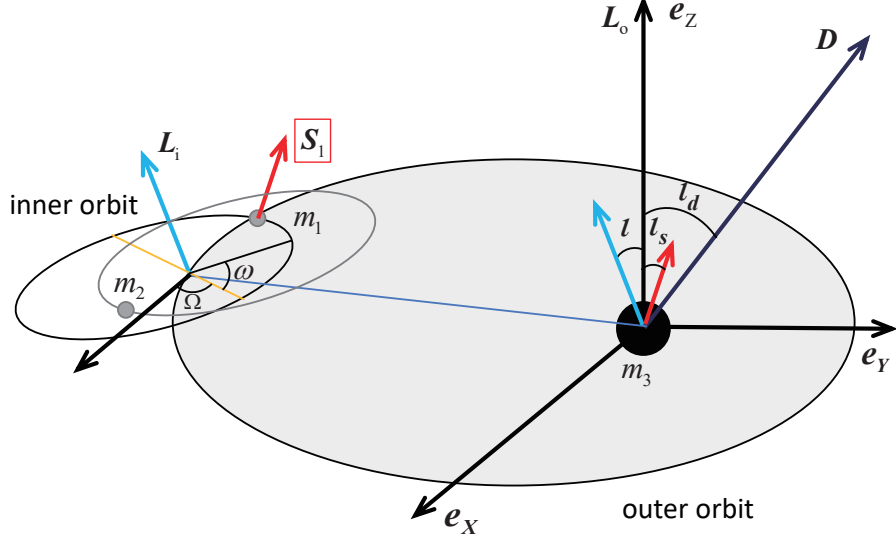


Figure 1. Geometric configuration of the hierarchical triple system where an NS binary orbits Sgr A*. The reference frame is chosen such that the outer orbital angular momentum \mathbf{L}_o aligns with the Z -axis. The inner binary orbital plane is tilted at inclination ι with respect to the outer orbit, with longitude of ascending node Ω and pericenter angle ω defining the orbital orientation. The vector \mathbf{S}_1 represents the primary NS spin. The detector inclination angle ι_d is defined between \mathbf{L}_o and \mathbf{D} , and the spin inclination angle ι_s between \mathbf{L}_o and \mathbf{S}_1 . Initially, both \mathbf{D} and \mathbf{S}_1 lie in the Y - Z plane, and their Y -components are positive.

\mathbf{D} projected onto the outer orbital plane as the Y -axis and the X -axis determined by the right-hand rule, such that \mathbf{S}_1 initially resides in the Y - Z plane and its Y -component is positive. Further details on the definitions of the inner orbital elements are provided in E. Poisson & C. M. Will (2014).

Following the Galactic Center binary population simulation results presented by H. Wang et al. (2021), the system parameters adopted in our analysis are set to $m_1 = m_2 = 1.4 \text{ M}_\odot$, $m_3 = 4 \times 10^6 \text{ M}_\odot$, $a_i = 0.012 \text{ AU}$, $e_i = 0.6$, $a_o = 2500 \text{ m}_3 \simeq 100 \text{ AU}$, and $e_o = 0.9$. The orbital periods of the inner and outer orbits are

$$P_i = 7 \text{ h} \left(\frac{2.8 \text{ M}_\odot}{m_1 + m_2} \right)^{1/2} \left(\frac{a_i}{0.012 \text{ AU}} \right)^{3/2}, \quad (1)$$

$$P_o = 0.5 \text{ yr} \left(\frac{m_3}{4 \times 10^6 \text{ M}_\odot} \right) \left(\frac{a_o}{2500 \text{ m}_3} \right)^{3/2}. \quad (2)$$

Sgr A* can perturb the inner orbit via the ZLK effect, in which oscillations in eccentricity and inclination arise on a timescale (B. Liu et al. 2019):

$$P_{\text{ZLK}} \sim 20 \text{ yr} \left(\frac{1 - e_o^2}{1 - 0.9^2} \right)^{3/2} \left(\frac{m_3}{4 \times 10^6 \text{ M}_\odot} \right)^2 \left(\frac{a_o}{2500 \text{ m}_3} \right)^3 \left(\frac{m_1 + m_2}{2.8 \text{ M}_\odot} \right)^{1/2} \left(\frac{a_i}{0.012 \text{ AU}} \right)^{-3/2}. \quad (3)$$

The inner binary undergoes periastron precession at 1st post-Newtonian (PN) order due to general relativity, with a precession period given by (H. P. Robertson 1938):

$$P_{1\text{PN}} \sim 220 \text{ yr} \left(\frac{1 - e_i^2}{1 - 0.6^2} \right) \left(\frac{m_1 + m_2}{2.8 \text{ M}_\odot} \right)^{-3/2} \left(\frac{a_i}{0.012 \text{ AU}} \right)^{5/2}. \quad (4)$$

The NS spin \mathbf{S}_1 is coupled to the inner orbital angular momentum \mathbf{L}_i through de-Sitter precession (1.5PN effect; e.g., B. M. Barker & R. F. O'Connell 1975) with a period

$$P_{S_1 L_i} \sim 260 \text{ yr} \left(\frac{1 - e_i^2}{1 - 0.6^2} \right) \left(\frac{a_i}{0.012 \text{ AU}} \right)^{5/2}. \quad (5)$$

The inner \mathbf{L}_i will undergoes a de Sitter-like precession around the outer \mathbf{L}_o (e.g., B. Liu et al. 2019; H. Yu & Y. Chen 2021) with a period

$$P_{L_i L_o} \sim 160 \text{ yr} \left(\frac{1 - e_o^2}{1 - 0.9^2} \right) \left(\frac{m_3}{4 \times 10^6 \text{ M}_\odot} \right) \left(\frac{a_o}{2500 m_3} \right)^{5/2}. \quad (6)$$

If Sgr A* possesses a spin angular momentum \mathbf{S}_3 with magnitude $S_3 = \chi_3 m_3^2$ (where χ_3 is the dimensionless spin parameter), then \mathbf{L}_o undergoes precession around \mathbf{S}_3 with a period (e.g., B. Liu & D. Lai 2022; Y. Fang et al. 2019)

$$P_{L_o S_3} \sim 2.8 \times 10^3 \text{ yr} \left(\frac{1 - e_o^2}{1 - 0.9^2} \right)^{3/2} \left(\frac{0.9}{\chi_3} \right) \left(\frac{m_3}{4 \times 10^6 \text{ M}_\odot} \right) \left(\frac{a_o}{2500 m_3} \right)^3. \quad (7)$$

The precession frequency of \mathbf{L}_i around \mathbf{S}_3 is one-fourth that of \mathbf{L}_o around \mathbf{S}_3 , thus the corresponding timescale is much longer (A. Laeuger et al. 2024).

The time it takes for the NS-NS to merge due to GW radiation can be written as (P. C. Peters 1964)

$$\tau_{\text{gw}} = 1.2 \times 10^8 \text{ yr} \frac{F(0.6)}{F(e_i)} \left(\frac{\mathcal{M}}{1.2 \text{ M}_\odot} \right)^{-5/3} \left(\frac{P_i}{7 \text{ h}} \right)^{8/3}, \quad (8)$$

with the eccentric orbital radiation factor $F(e) = (1 + \frac{73}{24}e^2 + \frac{37}{96}e^4)/(1 - e^2)^{7/2}$ and the inner binary chirp mass $\mathcal{M} = (m_1 m_2)^{3/5}/(m_1 + m_2)^{1/5}$. A large gravitational radiation decay timescale ensures the monochromaticity of harmonic frequencies.

Our analysis shows that, for the typical wide-orbit inner NS binaries taken from previous triple system simulations (H. Wang et al. 2021), ZLK timescales are much shorter than general relativistic precession timescales, establishing ZLK oscillations as the dominant dynamical mechanism.

3. DETECTABILITY OF NEUTRON STARS IN GALACTIC CENTER TRIPLES

The ZLK effect drives periodic oscillations in the orbital eccentricity and inclination of the compact inner NS binary, directly modulating its dual-line GW radiation. Previous investigations have concentrated on binary inspiral signatures, leaving continuous NS radiation significantly underexplored. Here, we address this gap by modeling individual NS gravitational radiation under the ZLK effect at the Galactic Center.

As a proof of concept, we adopt a widely used model for NS gravitational radiation (e.g., M. Maggiore 2007), in which the NS is asymmetric and rotates rapidly about one of its own principal axes of inertia, with the GW frequency being twice the rotation frequency. Our calculation can be easily extended to the precessing triaxial NSs (W.-F. Feng et al. 2025). Under the quadrupole approximation, the two GW polarizations in the source frame are given by

$$h_+(t) = \frac{4 I_3 \epsilon \Omega_r^2 [1 + \cos^2(\iota_d - \iota_s)] \cos(2t\Omega_r)}{2D}, \quad (9a)$$

$$h_\times(t) = \frac{4 I_3 \epsilon \Omega_r^2 \cos(\iota_d - \iota_s) \sin(2t\Omega_r)}{D}, \quad (9b)$$

where D is the distance between the source and the detector, Ω_r is the rotation frequency of the NS (not to confuse with angle Ω), ϵ is the equatorial ellipticity given by $(I_2 - I_1)/I_3$, and I_3 is the moment of inertia of the NS with respect to the principal axis aligned with the rotation axis, while the other two moments of inertia I_1 and I_2 are perpendicular to it, ι_d and ι_s denote the inclination angles of the detector and the NS spin relative to the reference-frame Z -axis, respectively.

A time-dependent GW strain at the detector is given by $h(t) = F_+(t)h_+(t) + F_\times(t)h_\times(t)$, where $F_+(t)$ and $F_\times(t)$ are the antenna pattern functions (P. Jaranowski et al. 1998). Due to the motion of Earth-based detectors relative to the Solar System Barycenter (SSB) and that of the NS about the triple system's barycenter, the observed continuous wave signal undergoes Doppler modulation from these two effects. As such, the GW angular frequency measured at the detector can be expressed as (e.g., W.-F. Feng et al. 2023b, 2025; P. B. Covas & A. M. Sintes 2019):

$$\Omega_r^d \approx \Omega_r \left(1 + \mathbf{n}_d \cdot \frac{d\mathbf{r}_{\text{ns}}}{dt} + \mathbf{n} \cdot \frac{d\mathbf{r}_d}{dt} \right). \quad (10)$$

Here \mathbf{n} and \mathbf{r}_d are the triple source direction vector and the detector position vector in the SSB frame (P. Jaranowski et al. 1998), $-\mathbf{n}_d = (0, \sin \iota_d, \cos \iota_d)$ is the SSB position vector in the triple source frame. The position vector \mathbf{r}_{ns} of the NS with spin \mathbf{S}_1 in this frame is given by

$$\mathbf{r}_{ns} = r_b \begin{pmatrix} \cos f_{t,o} \\ \sin f_{t,o} \\ 0 \end{pmatrix} + r_1 \begin{pmatrix} \cos(f_{t,i} + \omega) \cos \Omega - \cos \iota \sin(f_{t,i} + \omega) \sin \Omega \\ \cos \iota \cos \Omega \sin(f_{t,i} + \omega) + \cos(f_{t,i} + \omega) \sin \Omega \\ \sin \iota \sin(f_{t,i} + \omega) \end{pmatrix}, \quad (11)$$

where the first term on the right-hand side is the position vector of the binary barycenter in the triple source frame, with $r_b = a_o(1 - e_o^2)/(1 + e_o \cos f_{t,o})$. The second term denotes the position vector of the spinning NS in the binary barycenter frame, with $r_1 = a_1(1 - e_i^2)/(1 + e_i \cos f_{t,i})$. The semimajor axis of the NS orbit is $a_1 = m_2/(2\pi M/P_i)^{2/3}$. The true anomaly f_t can be expanded in terms of the mean anomaly $M_a = 2\pi(t - t_0)/P$ as follows (J. M. A. Danby 1988), $\cos f_t = -e + \frac{1-e^2}{e} \sum_{n=1}^{\infty} 2J_n(ne) \cos(nM_a)$, $\sin f_t = \sqrt{1-e^2} \sum_{n=1}^{\infty} \frac{2}{n} \frac{dJ_n(ne)}{de} \sin(nM_a)$. Note that P and e refer to the period and eccentricity of either the inner orbit or the outer orbit. Harmonics truncation is set to $n_{\max} = \lfloor 5(1+e)^{1/2}/(1-e)^{3/2} \rfloor$, ensuring that 99% of the signal power is retained (R. M. O’Leary et al. 2009; B. Mikoczi et al. 2012). Here, $\lfloor \cdot \rfloor$ is the floor function.

Based on the dynamical timescale analysis presented in Sec. 2, the effects of general relativity can be neglected. The outer orbital plane is chosen as the reference plane, the outer orbital elements are assumed to be constant, and the inner orbital elements can be solved via the following secular evolution equations at quadrupole order ($da_i/dt = 0$) (C. M. Will 2017):

$$\frac{de_i}{d\tau} = 5A \frac{e_i(1 - e_i^2)^{1/2}}{(1 - e_o^2)^{3/2}} \sin^2 \iota \sin \omega \cos \omega, \quad (12a)$$

$$\frac{d\iota}{d\tau} = -5A \frac{e_i^2 \sin \iota \cos \iota}{(1 - e_i^2)^{1/2}(1 - e_o^2)^{3/2}} \sin \omega \cos \omega, \quad (12b)$$

$$\frac{d\Omega}{d\tau} = -A \frac{(1 + 4e_i^2 - 5e_i^2 \cos^2 \omega)}{(1 - e_i^2)^{1/2}(1 - e_o^2)^{3/2}} \cos \iota, \quad (12c)$$

$$\frac{d\varpi}{d\tau} = A \frac{(1 - e_i^2)^{1/2}}{(1 - e_o^2)^{3/2}} [1 - \sin^2 \iota (4 - 5 \cos^2 \omega)], \quad (12d)$$

where a dimensionless time scaled by the inner orbital period $\tau \equiv t/P_i$, the coefficient $A \equiv (3\pi/2)m_3/(m_1 + m_2)(a_i/a_o)^3$, and the auxiliary variable is defined as $d\varpi/d\tau \equiv d\omega/d\tau + d\Omega/d\tau \cos \iota$. For simplicity, the effects of the octupole (vanishing for equal mass inner binaries) and hexadecapole order terms (C. M. Will 2017), the spin of the SMBH acting as the tertiary body (Y. Fang & Q.-G. Huang 2019), and the interactions with surrounding stars and gas (Y. Su et al. 2025) at the Galactic Center are all neglected in our work. The analytical solution based on the equivalent pendulum model, which is convenient for subsequent analysis, is derived in Appendix A.

The optimal signal-to-noise ratio (SNR) ρ_{NS} for the spinning NS with a monochromatic signal of GW frequency f is given by

$$\rho_{NS} \approx \sqrt{\frac{2}{S_n(f)} \int_0^{T_{\text{obs}}} h(t)^2 dt}. \quad (13)$$

Here, $S_n(f)$ denotes the noise power spectral density and T_{obs} is the observation time. Assuming the 40 km Cosmic Explorer design optimized for the low-frequency band (V. Srivastava et al. 2022), the instrumental noise spectral density depends on frequency and thus varies with NS spin period. We set $T_{\text{obs}} = 4$ yr, the polarization angle $\psi_p = \pi/4$, and the angular parameters associated with the detector are adopted as $\zeta = \pi/2$, $\lambda = 0.764$, $\gamma_o = 1.5$, and $\phi_r = \phi_o = 0$ (W.-F. Feng et al. 2025).

Figure 2 presents SNR contours for rapidly spinning NSs at the Galactic Center in the parameter space of spin period (P_s) and equatorial ellipticity (ϵ) for a 4-year observation of Cosmic Explorer, calculated for a fixed distance of $D = 8$ kpc, NS moment of inertia $I_3 = 2 \times 10^{38}$ kg m², and specific angular parameters (e.g., $\iota_s = \pi/12$ and $\iota_d = \pi/4$). The contours are consistent with the scaling of continuous GW amplitude with $\epsilon \Omega_r^2$ in Eq. (9). The gray region ($\rho_{NS} < 5$) represents parameter space below the detection threshold, while the green regions ($\rho_{NS} \geq 10$, up to $\rho_{NS} = 50$) denote robustly detectable signals. For example, an NS with a spin period of 10 ms can be detected down to

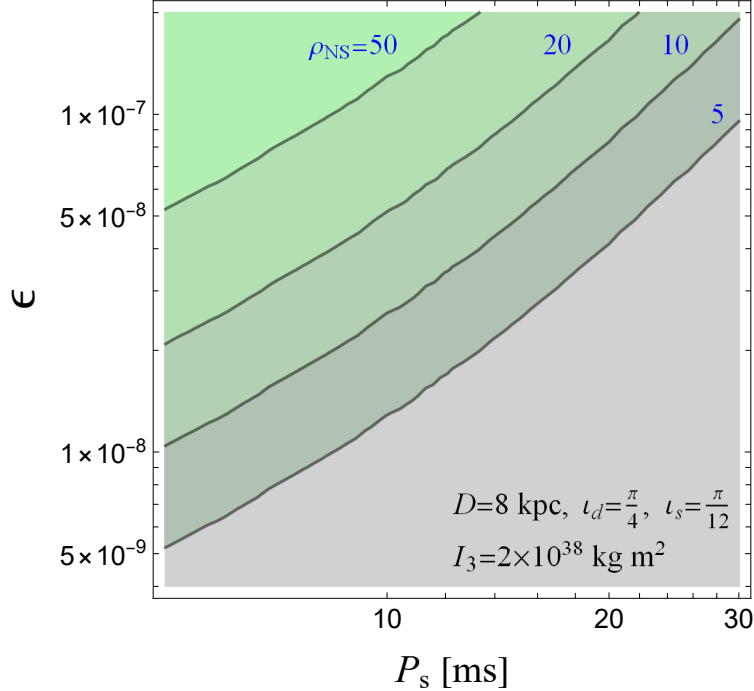


Figure 2. SNR contours for continuous GW detection from rapidly spinning NSs at the Galactic Center, shown in the spin period-equatorial ellipticity parameter space (P_s , ϵ) for a 4-year observation of Cosmic Explorer. The green shaded region indicates the detectable parameter space (assuming an SNR threshold of $\rho_{\text{NS}} = 5$). NSs spinning at $P_s = 10$ ms are detectable with ellipticities as small as $\epsilon \sim 10^{-8}$.

an ellipticity of $\epsilon \approx 10^{-8}$, whereas an NS with $P_s = 30$ ms requires $\epsilon \gtrsim 10^{-7}$ to reach the $\rho_{\text{NS}} = 5$ detection threshold. These results highlight the interplay between NS spin and ellipticity in determining detectability and demonstrate that rapidly spinning NSs with even modest ellipticities are promising targets for continuous-wave detection with Cosmic Explorer in the Galactic Center.

4. ZLK EFFECT-INDUCED DUAL-LINE GRAVITATIONAL RADIATION

The SNR for an inspiraling NS-NS system to be detected by space-borne GW observatories, characterized by an effective noise power spectral density $S_n(f)$, can be approximated as follows (see [H. Wang et al. 2021](#) and references therein):

$$\rho_{\text{NS-NS}}(e_i, T_{\text{obs}}) \approx \frac{32\sqrt{2}}{5} \frac{m_1 m_2}{a_i D} \sqrt{0.886 T_{\text{obs}} \sum_{n=1}^{n_{\text{max}}} \frac{g(n, e_i)}{n^2 S_n(f_n)}}, \quad (14)$$

where $f_n = n/P_i$ denotes the n -th orbital frequency harmonic, and $g(n, e_i)$ is the radiation power factor for the n -th harmonic defined via the Bessel functions of the first kind ([P. C. Peters & J. Mathews 1963](#)).

For isolated NS-NS systems without the ZLK effect [neglecting the variation of e_i in Eq. (14)], the $a_i - (1 - e_i)$ parameter space for LISA detectability naturally divides into three distinct regions in Fig. 3: the upper white region (unresolvable), the green diagonal band (detectable), and the lower gray region (absent). The physical origin of this division reflects GW-driven evolution and source population statistics. Gravitational radiation causes orbital decay, reducing both semimajor axis and eccentricity ([P. C. Peters 1964](#)), which concentrates sources toward larger a_i and higher e_i values ([W.-F. Feng et al. 2023a, 2024; K. Kyutoku & N. Seto 2016](#)). This evolutionary bias creates three regions: (1) The white region contains wide-orbit systems that emit GWs below the detection SNR threshold of $\rho_{\text{NS-NS}} = 5$, forming an unresolved background; (2) The green band represents the optimal detection window where binary inspirals produce sufficiently strong signals, e.g., $\rho_{\text{NS-NS}} = 5-40$ as found in simulations of [H. Wang et al. \(2021\)](#); (3) The gray region is depleted of sources because tight binaries merge rapidly, spending minimal time in this high frequency regime—consistent with simulations of [H. Wang et al. \(2021\)](#) showing no systems exceeding SNR ~ 40 .

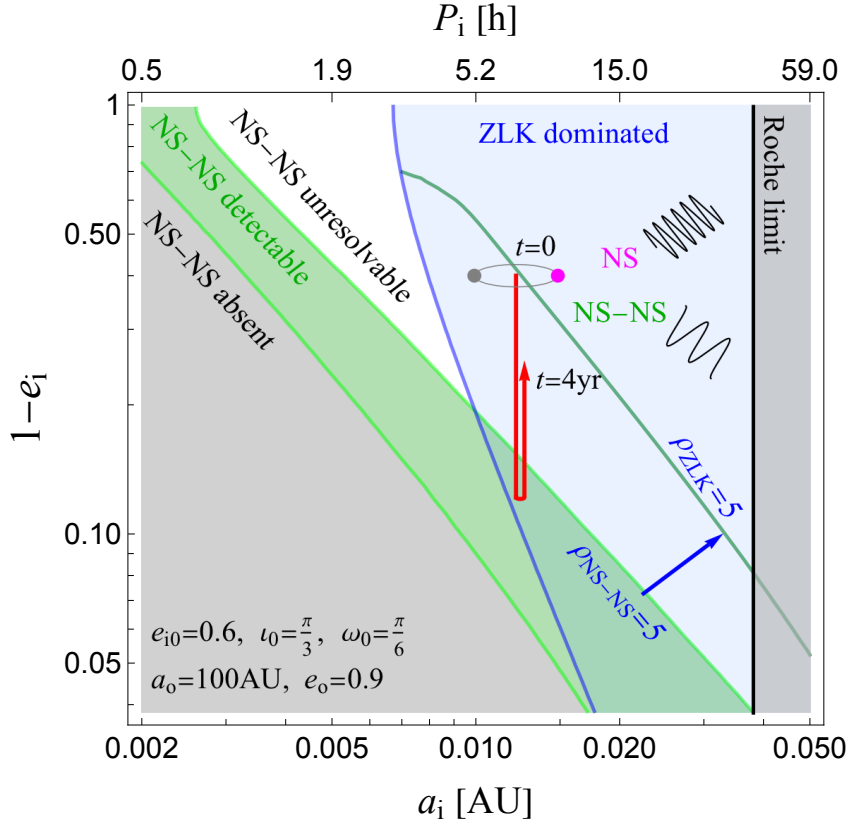


Figure 3. Dual-line gravitational radiation excitation through the ZLK effect for the Galactic Center NS-NS systems. Green contours show LISA-detectable systems without the ZLK effect, bounded by $\rho_{\text{NS-NS}} = 5$ (right) and $\rho_{\text{NS-NS}} = 40$ (left) in the $a_i - (1 - e_i)$ parameter space. The light blue region indicates ZLK dominance, exemplified by a system with $e_{i0} = 0.6$ and $P_i = 7$ h. The magenta point represents a rapidly spinning NS component detectable by Cosmic Explorer (Fig. 2). Without ZLK, this system has $\rho_{\text{NS-NS}} = 0.16$ (undetectable), but ZLK-driven eccentricity oscillations boost the SNR to 5.5 over 4 years. The dark green contour shows the ZLK-modified SNR threshold $\rho_{\text{ZLK}} = 5$, which extends into regions of larger orbital separation and lower eccentricity than the standard detection boundary. Monte Carlo sampling indicates that this parameter-space expansion increases the number of detectable sources by threefold. ZLK oscillations therefore promote wide binaries from unresolvable backgrounds into LISA’s detection window, substantially improving dual-line prospects and establishing the ZLK effect as a viable formation channel for Galactic Center dual-line systems.

This stable three-region structure changes significantly when NS-NS systems are embedded in hierarchical triple systems with Sgr A*. The ZLK effect introduces periodic modulations in orbital eccentricity, allowing systems to migrate between detection regimes over evolutionary timescales. ZLK oscillations dominate over general relativistic precession in the light blue region of Fig. 3. Neglecting the e_i dependence and order-unity factors, this is approximately equivalent to $P_{\text{ZLK}} < P_{1\text{PN}}$, which corresponds to the hierarchical triple criterion (O. Blaes et al. 2002):

$$\frac{a_o^3}{a_i^3} < \frac{3m_3 a_i (1 - e_i^2)^{3/2}}{4(m_1 + m_2)^2 (1 - e_o^2)^{3/2}}. \quad (15)$$

In ZLK-dominated systems, orbital eccentricity varies significantly over the observation period, requiring a time-dependent analysis. We discretize the total observation time T_{obs} into N_{seg} segments of duration ΔT , treating the eccentricity as constant ($e_{i,j}$) within each interval. The integrated SNR is computed by summing the squared SNR contributions from each segment:

$$\rho_{\text{ZLK}} \approx \sqrt{\sum_{j=1}^{N_{\text{seg}}} \rho_{\text{NS-NS}}^2(e_{i,j}, \Delta T)}. \quad (16)$$

Figure 3 demonstrates the dual-line gravitational radiation excitation through the ZLK effect. In the ZLK-dominated regime, we examine a representative system with initial parameters matching the most probable system in H. Wang

et al. (2021): $e_i = 0.6$, $P_i = 7$ h (binary labeled at $t = 0$), and a rapidly spinning NS (magenta dot) detectable by Cosmic Explorer (Fig. 2). The ZLK enhancement is dramatic: without ZLK effects, this system yields $\rho_{\text{NS-NS}} = 0.16$ [Eq. (14)], remaining undetectable by LISA. However, ZLK-driven eccentricity oscillations over 4 years boost the SNR to $\rho_{\text{ZLK}} = 5.5$ [Eq. (16)], crossing the detection threshold.

We find that the ZLK-modified SNR contour ($\rho_{\text{ZLK}} = 5$, dark green) extends to larger orbital separations and lower eccentricities, substantially increasing the detectable population. To quantify this enhancement, we perform Monte Carlo sampling of the inner orbital parameters: the semimajor axis a_i is drawn from a distribution $\propto a_i^4$ (via inverse-transform sampling; W.-F. Feng et al. (2024)) and the eccentricity from a thermal law $p(e_i) = 2e_i$ (D. C. Heggie 1975). For each realization, we count Monte Carlo points that fall within the detection region (bounded by the threshold contours, ZLK-dominated boundary, and the vertical Roche-limit line defined below), and derive an area ratio from the point counts. This procedure indicates that allowing for ZLK-induced excursions into wider separations and lower eccentricities increases the detectable parameter space by ~ 3 for both uniform and thermal eccentricity prescriptions.

As an order-of-magnitude feasibility estimate, we then write

$$N_d \sim N_b \times f_{100\text{au}} \times f_{\text{ns}} \times f_{\text{zlk}}, \quad (17)$$

where $N_b \sim 0.6\text{--}6$ denotes the number of LISA-detectable NS binaries assuming constant eccentricity during the observation period [Eq. (14)], $f_{100\text{au}} \sim 0.1$ represents the fraction of binaries within 100 AU of Sgr A* (assuming log-uniform outer orbits to 0.1 pc), and $f_{\text{ns}} \sim 0.2\text{--}0.6$ is the fraction of NS components detectable by Cosmic Explorer (W.-F. Feng & L. Shao 2025). Using the Monte Carlo area ratio as the ZLK enhancement factor ($f_{\text{zlk}} \sim 3$) raises the expected dual-line yield from $\mathcal{O}(0.01\text{--}0.4)$ without the ZLK effect to $\mathcal{O}(0.03\text{--}1)$ in 4 years. These order-of-magnitude results indicate that ZLK dynamics constitute a viable channel for producing Galactic Center dual-line systems.

Note that the binary considered in the above example satisfies the stability criterion requiring that the inner binary not cross the Roche limit of the Sgr A* at its pericenter (B.-M. Hoang et al. 2019; S. Naoz & J. Silk 2014), namely $a_i/a_o < [(m_1 + m_2)/(3m_3)]^{1/3} (1 - e_o)/(1 + e_i)$. Additionally, it satisfies the condition for the applicability of the orbit-averaged approximation, valid for a stationary outer perturber and instantaneous quadrupole torque (F. Antonini et al. 2014), as $\sqrt{1 - e_i} > 5\pi m_3/(m_1 + m_2) a_i^3/[a_o(1 - e_o)]^3$. To facilitate the visualization of the eccentricity evolution path, we intentionally introduce a small change in the inner orbital semimajor axis a_i over a 4-year observation period, manifested as the non-overlapping of the two red vertical lines in Fig. 3. Although 1PN precession is enhanced by a factor of $(1 - e_i^2)^{-1}$ [see Eq. (4)] during eccentricity excitation, it remains insufficient to suppress ZLK oscillations in the light blue region where most Galactic Center sources reside.

5. DISCUSSION AND CONCLUSIONS

In this work, we demonstrate that the ZLK effect in Galactic Center hierarchical triples can dramatically enhance the prospects for dual-line GW detection. Our dynamical analysis reveals that ZLK oscillations dominate over general relativistic precession for wide NS-NS binaries, enabling significant orbital modulations over multi-year timescales. This mechanism operates through complementary pathways: ZLK-driven eccentricity oscillations promote wide systems from below LISA sensitivity into the detectable regime, while rapidly spinning NSs in these binaries simultaneously emit continuous GWs accessible to Cosmic Explorer. The resulting dual-line detectability represents a substantial enhancement over isolated binary evolution.

Quantitatively, we find that the ZLK-modified detection threshold extends to larger orbital separations and lower eccentricities, Monte Carlo sampling indicates this expansion increases the detectable population by ~ 3 . Our fiducial system illustrates this effect, evolving from undetectable ($\rho_{\text{NS-NS}} = 0.16$) to detectable ($\rho_{\text{ZLK}} = 5.5$) over a 4-year observation. An order-of-magnitude feasibility estimate therefore raises the expected yield to $\mathcal{O}(0.03\text{--}1)$ dual-line sources per 4-year mission, compared with $\mathcal{O}(0.01\text{--}0.4)$ without ZLK enhancement—transforming the observational outlook from challenging to probable.

Our estimates rely on simplified population simulations and assume favorable system configurations. Future studies should incorporate more realistic stellar-evolution models, detailed ZLK modeling that includes high-order effects, and comprehensive population synthesis to refine these predictions.

ZLK oscillations thus provide a promising formation channel for Galactic Center dual-line sources, offering transformative scientific opportunities beyond detection enhancement. Simultaneous multi-band observations would place

high-precision constraints on NS equations of state while encoding Galactic Center dynamics, establishing a powerful pathway for dual-line GW astronomy that bridges compact object physics and Galactic structure.

ACKNOWLEDGMENTS

We thank Smadar Naoz, Xian Chen, Yan Wang, Haoran Di, Hao Wang, Zhao Li, and Jiang-Chuan Yu for helpful discussions. W.-F.F. is supported by the China Postdoctoral Science Foundation under Grant No. 2025M783222, and the National Natural Science Foundation of China under Grant No. 12447109. B.L. acknowledges support from the National Natural Science Foundation of China (Grant No. 12433008) and National Key Research and Development Program of China (No. 2023YFB3002502). L.S. acknowledges support from the Beijing Natural Science Foundation (1242018), the National Natural Science Foundation of China (12573042), the National SKA Program of China (2020SKA0120300), and the Max Planck Partner Group Program funded by the Max Planck Society.

APPENDIX

A. ANALYTICAL SOLUTION FOR ECCENTRICITY AND INCLINATION

The quadrupole ZLK mechanism for a test particle exhibits behavior analogous to that of a mechanical pendulum (R. D. Basha et al. 2025), which is described by the following equation:

$$\ddot{\theta}_K + \omega_K^2 \sin \theta_K = 0, \quad (A1)$$

where θ_K denotes the pendulum angle, and ω_K is a constant corresponding to the angular frequency in small-amplitude oscillations. In the context of two conserved quantities of motion: $j_z = (1 - e_i^2)^{1/2} \cos \iota$ and $C_K = e_i^2 (1 - 5 \sin^2 \iota \sin^2 \omega/2)$, this analogy is explicitly expressed as:

$$\dot{\theta}_K = \frac{3}{2} \sqrt{15} e_i \sin \iota \sin \omega, \quad (A2a)$$

$$\omega_K^2 = \frac{9}{8} \left[(3 - 5j_z^2 - 2C_K)^2 + 24C_K \right]^{1/2}. \quad (A2b)$$

The normalized energy of the pendulum (a dimensionless constant of motion) is given by:

$$E_K = \frac{\dot{\theta}_K^2}{2\omega_K^2} + 1 - \cos \theta_K = 1 + \frac{9}{8\omega_K^2} (3 - 5j_z^2 - 8C_K). \quad (A3)$$

The exact solution for the angular displacement $\theta_K(t)$ under the initial conditions, $\theta_K(0) = \theta_{K0}$ and $\dot{\theta}_K(0) = \omega_{K0}$, is given by:

$$\theta_K(t) = 2 \arcsin [k \cdot \text{sn}(\pm \omega_K t + \phi_{K0}, k)], \quad (A4)$$

where $\text{sn}(u, k)$ denotes the Jacobian elliptic sine function. The modulus k and initial phase constant ϕ_{K0} of this elliptic function are defined as:

$$k = \sin \left(\frac{\theta_{K\max}}{2} \right), \quad \phi_{K0} = \text{sn}^{-1} \left(\frac{\sin(\theta_{K0}/2)}{k}, k \right), \quad (A5)$$

with $\theta_{K\max}$ representing the maximum angular displacement of the pendulum-like motion. For pendulum libration ($C_K > 0$), $\theta_{K\max} = \arccos(1 - E_K)$. The sign “ \pm ” in the argument of $\text{sn}(u, k)$ is determined by the sign of ω_{K0} .

The analytical solution for the inner eccentricity reads:

$$e_i = [l_K E_K + C_K - l_K(1 - \cos \theta_K)]^{1/2}, \quad (A6)$$

where $l_K = 4\omega_K^2/27$ denotes the equivalent length of the pendulum (a derived constant of the system). Correspondingly, the analytical solution for the inclination is given by:

$$\iota = \arccos \left[j_z (1 - e_i^2)^{-1/2} \right]. \quad (A7)$$

REFERENCES

Abbott, B. P., et al. 2017, Phys. Rev. Lett., 119, 161101, doi: [10.1103/PhysRevLett.119.161101](https://doi.org/10.1103/PhysRevLett.119.161101)

Akiyama, K., et al. 2022a, Astrophys. J. Lett., 930, L12, doi: [10.3847/2041-8213/ac6674](https://doi.org/10.3847/2041-8213/ac6674)

Akiyama, K., et al. 2022b, Astrophys. J. Lett., 930, L17, doi: [10.3847/2041-8213/ac6756](https://doi.org/10.3847/2041-8213/ac6756)

Alexander, T. 2005, Phys. Rept., 419, 65, doi: [10.1016/j.physrep.2005.08.002](https://doi.org/10.1016/j.physrep.2005.08.002)

Alexander, T., & Pfuhl, O. 2014, Astrophys. J., 780, 148, doi: [10.1088/0004-637X/780/2/148](https://doi.org/10.1088/0004-637X/780/2/148)

Amaro-Seoane, P., et al. 2017, <https://arxiv.org/abs/1702.00786>

Antonini, F., Murray, N., & Mikkola, S. 2014, Astrophys. J., 781, 45, doi: [10.1088/0004-637X/781/1/45](https://doi.org/10.1088/0004-637X/781/1/45)

Barker, B. M., & O'Connell, R. F. 1975, Phys. Rev. D, 12, 329, doi: [10.1103/PhysRevD.12.329](https://doi.org/10.1103/PhysRevD.12.329)

Basha, R. D., Klein, Y. Y., & Katz, B. 2025, Monthly Notices of the Royal Astronomical Society: Letters, 541, L43, doi: [10.1093/mnrasl/sla050](https://doi.org/10.1093/mnrasl/sla050)

Blaes, O., Lee, M. H., & Socrates, A. 2002, Astrophys. J., 578, 775, doi: [10.1086/342655](https://doi.org/10.1086/342655)

Boehle, A., et al. 2016, Astrophys. J., 830, 17, doi: [10.3847/0004-637x/830/1/17](https://doi.org/10.3847/0004-637x/830/1/17)

Chandramouli, R. S., & Yunes, N. 2022, Phys. Rev. D, 105, 064009, doi: [10.1103/PhysRevD.105.064009](https://doi.org/10.1103/PhysRevD.105.064009)

Chen, W.-C. 2021, Phys. Rev. D, 103, 103004, doi: [10.1103/PhysRevD.103.103004](https://doi.org/10.1103/PhysRevD.103.103004)

Chu, D. S., et al. 2018, Astrophys. J., 854, 12, doi: [10.3847/1538-4357/aaa3eb](https://doi.org/10.3847/1538-4357/aaa3eb)

Covas, P. B., & Sintes, A. M. 2019, Phys. Rev. D, 99, 124019, doi: [10.1103/PhysRevD.99.124019](https://doi.org/10.1103/PhysRevD.99.124019)

Danby, J. M. A. 1988, Fundamentals of celestial mechanics (Richmond, Virginia, United States of America: Willmann-Bell Inc.)

Fang, Y., Chen, X., & Huang, Q.-G. 2019, The Astrophysical Journal, 887, 210, doi: [10.3847/1538-4357/ab510e](https://doi.org/10.3847/1538-4357/ab510e)

Fang, Y., & Huang, Q.-G. 2019, Phys. Rev. D, 99, 103005, doi: [10.1103/PhysRevD.99.103005](https://doi.org/10.1103/PhysRevD.99.103005)

Feng, W.-F., Chen, J.-W., Liu, T., Wang, Y., & Mohanty, S. D. 2024, Phys. Rev. D, 109, 043033, doi: [10.1103/PhysRevD.109.043033](https://doi.org/10.1103/PhysRevD.109.043033)

Feng, W.-F., Chen, J.-W., Wang, Y., Mohanty, S. D., & Shao, Y. 2023a, Phys. Rev. D, 107, 103035, doi: [10.1103/PhysRevD.107.103035](https://doi.org/10.1103/PhysRevD.107.103035)

Feng, W.-F., Liu, T., Chen, J.-W., Wang, Y., & Mohanty, S. D. 2023b, Phys. Rev. D, 108, 063035, doi: [10.1103/PhysRevD.108.063035](https://doi.org/10.1103/PhysRevD.108.063035)

Feng, W.-F., Liu, T., Wang, Y., & Shao, L. 2025, Phys. Rev. D, 111, 023053, doi: [10.1103/PhysRevD.111.023053](https://doi.org/10.1103/PhysRevD.111.023053)

Feng, W.-F., & Shao, L. 2025, Phys. Rev. D, 112, 043023, doi: [10.1103/bqtw-vdws](https://doi.org/10.1103/bqtw-vdws)

Ghez, A. M., Becklin, E., Duchene, G., et al. 2003, Astron. Nachr., 324, S1, doi: [10.1002/asna.200385103](https://doi.org/10.1002/asna.200385103)

Ghez, A. M., Salim, S., Hornstein, S. D., et al. 2005, Astrophys. J., 620, 744, doi: [10.1086/427175](https://doi.org/10.1086/427175)

Ghez, A. M., et al. 2008, Astrophys. J., 689, 1044, doi: [10.1086/592738](https://doi.org/10.1086/592738)

Gillessen, S., Eisenhauer, F., Trippe, S., et al. 2009, Astrophys. J., 692, 1075, doi: [10.1088/0004-637X/692/2/1075](https://doi.org/10.1088/0004-637X/692/2/1075)

Gillessen, S., et al. 2012, Nature, 481, 51, doi: [10.1038/nature10652](https://doi.org/10.1038/nature10652)

Hees, A., et al. 2017, Phys. Rev. Lett., 118, 211101, doi: [10.1103/PhysRevLett.118.211101](https://doi.org/10.1103/PhysRevLett.118.211101)

Heggie, D. C. 1975, Mon. Not. Roy. Astron. Soc., 173, 729, doi: [10.1093/mnras/173.3.729](https://doi.org/10.1093/mnras/173.3.729)

Hoang, B.-M., Naoz, S., Kocsis, B., Farr, W., & McIver, J. 2019, Astrophys. J. Lett., 875, L31, doi: [10.3847/2041-8213/ab14f7](https://doi.org/10.3847/2041-8213/ab14f7)

Hoang, B.-M., Naoz, S., & Kremer, K. 2020, Astrophys. J., 903, 8, doi: [10.3847/1538-4357/abb66a](https://doi.org/10.3847/1538-4357/abb66a)

Hopman, C. 2009, Astrophys. J., 700, 1933, doi: [10.1088/0004-637X/700/2/1933](https://doi.org/10.1088/0004-637X/700/2/1933)

Hu, W.-R., & Wu, Y.-L. 2017, Natl. Sci. Rev., 4, 685, doi: [10.1093/nsr/nwx116](https://doi.org/10.1093/nsr/nwx116)

Hu, Z., & Shao, L. 2024, Phys. Rev. Lett., 133, 231402, doi: [10.1103/PhysRevLett.133.231402](https://doi.org/10.1103/PhysRevLett.133.231402)

Jaranowski, P., Krolak, A., & Schutz, B. F. 1998, Phys. Rev. D, 58, 063001, doi: [10.1103/PhysRevD.58.063001](https://doi.org/10.1103/PhysRevD.58.063001)

Knee, A. M., McIver, J., Naoz, S., et al. 2024, Astrophys. J. Lett., 971, L38, doi: [10.3847/2041-8213/ad6a10](https://doi.org/10.3847/2041-8213/ad6a10)

Kozai, Y. 1962, Astron. J., 67, 591, doi: [10.1086/108790](https://doi.org/10.1086/108790)

Kyutoku, K., & Seto, N. 2016, Mon. Not. Roy. Astron. Soc., 462, 2177, doi: [10.1093/mnras/stw1767](https://doi.org/10.1093/mnras/stw1767)

Laeuger, A., Seymour, B., Chen, Y., & Yu, H. 2024, Phys. Rev. D, 109, 064086, doi: [10.1103/PhysRevD.109.064086](https://doi.org/10.1103/PhysRevD.109.064086)

Lidov, M. L. 1962, Planet. Space Sci., 9, 719, doi: [10.1016/0032-0633\(62\)90129-0](https://doi.org/10.1016/0032-0633(62)90129-0)

Liu, B., & Lai, D. 2022, Astrophys. J., 924, 127, doi: [10.3847/1538-4357/ac3aef](https://doi.org/10.3847/1538-4357/ac3aef)

Liu, B., Lai, D., & Wang, Y.-H. 2019, Astrophys. J. Lett., 883, L7, doi: [10.3847/2041-8213/ab40c0](https://doi.org/10.3847/2041-8213/ab40c0)

Luo, J., et al. 2016, Class. Quant. Grav., 33, 035010, doi: [10.1088/0264-9381/33/3/035010](https://doi.org/10.1088/0264-9381/33/3/035010)

Maggiore, M. 2007, Gravitational Waves. Vol. 1: Theory and Experiments (Oxford University Press), doi: [10.1093/acprof:oso/9780198570745.001.0001](https://doi.org/10.1093/acprof:oso/9780198570745.001.0001)

Mikoczi, B., Kocsis, B., Forgacs, P., & Vasuth, M. 2012, Phys. Rev. D, 86, 104027, doi: [10.1103/PhysRevD.86.104027](https://doi.org/10.1103/PhysRevD.86.104027)

Naoz, S. 2016, Ann. Rev. Astron. Astrophys., 54, 441, doi: [10.1146/annurev-astro-081915-023315](https://doi.org/10.1146/annurev-astro-081915-023315)

Naoz, S., & Silk, J. 2014, The Astrophysical Journal, 795, 102, doi: [10.1088/0004-637X/795/2/102](https://doi.org/10.1088/0004-637X/795/2/102)

O’Leary, R. M., Kocsis, B., & Loeb, A. 2009, Mon. Not. Roy. Astron. Soc., 395, 2127, doi: [10.1111/j.1365-2966.2009.14653.x](https://doi.org/10.1111/j.1365-2966.2009.14653.x)

Peters, P. C. 1964, Phys. Rev., 136, B1224, doi: [10.1103/PhysRev.136.B1224](https://doi.org/10.1103/PhysRev.136.B1224)

Peters, P. C., & Mathews, J. 1963, Phys. Rev., 131, 435, doi: [10.1103/PhysRev.131.435](https://doi.org/10.1103/PhysRev.131.435)

Poisson, E., & Will, C. M. 2014, Gravity: Newtonian, post-Newtonian, Relativistic (Cambridge, England: Cambridge University Press)

Punturo, M., Abernathy, M., & et al. 2010, Class. Quantum Grav., 27, 194002, doi: [10.1088/0264-9381/27/19/194002](https://doi.org/10.1088/0264-9381/27/19/194002)

Randall, L., & Xianyu, Z.-Z. 2019, <https://arxiv.org/abs/1902.08604>

Robertson, H. P. 1938, Annals of Mathematics, 39, 101

Rodriguez, D. R., & Zuckerman, B. 2012, Astrophys. J., 745, 147, doi: [10.1088/0004-637X/745/2/147](https://doi.org/10.1088/0004-637X/745/2/147)

Sedda, M. A. 2020, Commun. Phys., 3, 43, doi: [10.1038/s42005-020-0310-x](https://doi.org/10.1038/s42005-020-0310-x)

Shao, L., Wex, N., & Kramer, M. 2018, Phys. Rev. Lett., 120, 241104, doi: [10.1103/PhysRevLett.120.241104](https://doi.org/10.1103/PhysRevLett.120.241104)

Srivastava, V., Davis, D., Kuns, K., et al. 2022, Astrophys. J., 931, 22, doi: [10.3847/1538-4357/ac5f04](https://doi.org/10.3847/1538-4357/ac5f04)

Stephan, A. P., Naoz, S., Ghez, A. M., et al. 2016, Mon. Not. Roy. Astron. Soc., 460, 3494, doi: [10.1093/mnras/stw1220](https://doi.org/10.1093/mnras/stw1220)

Stephan, A. P., Naoz, S., Ghez, A. M., et al. 2019, Astrophys. J., 878, 58, doi: [10.3847/1538-4357/ab1e4d](https://doi.org/10.3847/1538-4357/ab1e4d)

Su, Y., Rowan, C., & Rozner, M. 2025, Mon. Not. Roy. Astron. Soc., 543, 1864, doi: [10.1093/mnras/staf1592](https://doi.org/10.1093/mnras/staf1592)

Suvorov, A. G. 2021, Mon. Not. Roy. Astron. Soc., 503, 5495, doi: [10.1093/mnras/stab825](https://doi.org/10.1093/mnras/stab825)

Tauris, T. M. 2018, Phys. Rev. Lett., 121, 131105, doi: [10.1103/PhysRevLett.121.131105](https://doi.org/10.1103/PhysRevLett.121.131105)

Tsang, D. 2013, Astrophys. J., 777, 103, doi: [10.1088/0004-637X/777/2/103](https://doi.org/10.1088/0004-637X/777/2/103)

von Zeipel, H. 1910, Astronomische Nachrichten, 183, 345, doi: [10.1002/asna.19091832202](https://doi.org/10.1002/asna.19091832202)

Wang, H., Stephan, A. P., Naoz, S., Hoang, B.-M., & Breivik, K. 2021, Astrophys. J., 917, 76, doi: [10.3847/1538-4357/ac088d](https://doi.org/10.3847/1538-4357/ac088d)

Will, C. M. 2017, Phys. Rev. D, 96, 023017, doi: [10.1103/PhysRevD.96.023017](https://doi.org/10.1103/PhysRevD.96.023017)

Yu, H., & Chen, Y. 2021, Phys. Rev. Lett., 126, 021101, doi: [10.1103/PhysRevLett.126.021101](https://doi.org/10.1103/PhysRevLett.126.021101)

Yu, J.-C., Cao, Y., Hu, Z., & Shao, L. 2025, <https://arxiv.org/abs/2510.22573>

Zhang, F., Shao, L., & Zhu, W. 2019, Astrophys. J., 877, 87, doi: [10.3847/1538-4357/ab1b28](https://doi.org/10.3847/1538-4357/ab1b28)